Theory and predictions for finite-amplitude waves in two-dimensional plane Poiseuille flow

Dwight Barkley[a)]
Applied Mathematics, California Institute of Technology, Pasadena, California 91125

(Received 3 November 1989; accepted 26 February 1990)

It has been found by Pugh and Saffman [J. Fluid Mech. **194**, 295 (1988)] that in a two-dimensional channel, the stability of finite-amplitude steady waves to modulated waves can depend on the boundary conditions imposed on the flow. In particular, near the limit point in Reynolds number, stability can depend on whether the flux or the mean pressure gradient is prescribed for the flow. Here a continuous range of intermediate boundary conditions is defined and studied using bifurcation theory. Based only on previous numerical solutions to the Navier–Stokes equations at constant mean flux and constant mean pressure gradient, it is shown that the finite-amplitude steady waves must have a double-zero eigenvalue at some intermediate boundary condition. From this a unifying picture emerges for the dynamics near the limit point in Reynolds number and specific predictions are made for finite-amplitude solutions to the Navier–Stokes equations. These predictions include the existence of a homoclinic orbit and a degenerate Hopf bifurcation.

I. INTRODUCTION

In this paper we use bifurcation theory to provide insight into the stability of finite-amplitude Tollmien–Schlichting waves in two-dimensional (2-D) plane Poiseuille flow. While three-dimensional (secondary) instabilities of finite-amplitude waves have received most of the attention in recent years,[1,2] there are aspects of the 2-D stability problem that have not yet been completely understood. In particular, it has recently been found[3,4] that, near the limit point in Reynolds number, the stability of steady waves can depend on the longitudinal boundary conditions imposed on the flow. In addition, depending on the boundary conditions, modulated waves may bifurcate from the steady waves near the limit-point. We seek to explain, within a bifurcation-theoretic framework, the relationship between the modulated waves and change of stability at the limit point of steady waves.

Let us first describe the situation in more detail. Figure 1(a) shows a fixed-wavenumber bifurcation diagram for longitudinal boundary conditions such that the flux through the channel is time independent. This bifurcation diagram is based on the numerical computations of Pugh and Saffman[3] and Soibelman,[4] but similar diagrams for steady waves have been obtained by many authors, notably Zahn *et al.*[5] and Herbert.[6] For the wavenumber shown, the parabolic velocity profile is linearly stable for all Reynolds numbers. There is a branch of 2-D traveling waves that becomes stable at the "nose" or limit point in Reynolds number. (As we shall limit our considerations to 2-D phenomena in this paper, all statements of stability implicitly refer to 2-D stability.) These waves are seen as time independent, i.e., steady, in a frame of reference moving with the wave speed.

The situation is different for boundary conditions such that the mean pressure gradient is time independent [Fig. 1(b)]. In this case, the steady waves do not stabilize at the limit point but become unstable to second a eigenmode, i.e., a second eigenvalue becomes positive at the limit point. The steady waves stabilize at a Hopf bifurcation on the upper branch and issuing from this Hopf bifurcation is a branch of modulated waves. The modulated waves are analogous to the modulated waves in Couette–Taylor flow;[7] they are seen as quasiperiodic in laboratory-fixed coordinates and as periodic in a frame uniformly translating with the appropriate speed.

Soibelman[4] has recently numerically computed the branch of modulated waves and the qualitative character is shown in Fig. 1(b). The branch first decreases in Reynolds number, and presumably the modulated waves are stable. Soibelman did not obtain the stability of the modulated waves because of the computational expense involved; the stability indicated in the figure is conjecture based on the theory of the Hopf bifurcation.[8,9] The modulated-wave branch itself has a limit point, where the modulated waves presumably become unstable. The fate of the modulated waves with increasing Reynolds number is not resolved by Soibelman's computations. Because of the number of modes required to obtain quantitative results at the Hopf bifurcation and at the limit point for the modulated waves, the Reynolds numbers for these bifurcations are not known precisely; however, $Re_P \simeq 3800$ is probably a good approximation to the Reynolds number for the Hopf bifurcation. (The notation for the Reynolds numbers is discussed in Sec. II.) Hopf bifurcations of the steady-wave branch at higher Reynolds numbers have also been found[3,4,10] and studied elsewhere.[10] We shall not consider these bifurcations here.

Our approach to understanding the behavior depicted in Fig. 1 is to introduce an additional parameter, μ, which interpolates between the constant-flux and constant-mean

[a)]Present address: Program in Applied and Computational Mathematics, 202 Fine Hall, Princeton University, Princeton, New Jersey 08544.

 0899-8213/90/060955-16$02.00

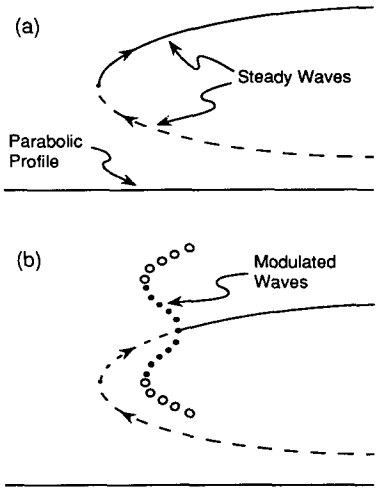

FIG. 1. Schematic bifurcation diagrams based on numerical studies of the Navier–Stokes equations in Refs. 3 and 4. The horizontal coordinate is Reynolds number, the vertical coordinate is a norm measuring the amplitude of states. The streamwise wavenumber is $\alpha = 1.1$, nondimensionalized by the channel half-width; for this wavenumber the parabolic velocity profile is linearly stable for all Reynolds numbers. Diagrams are shown for two different longitudinal boundary conditions: (a) boundary conditions such that the flux through the channel is time independent. The solid curve denotes stable steady waves, the dashed curve denotes unstable steady waves with one positive eigenvalue. The Reynolds number of the limit point is $\mathrm{Re}_Q \simeq 2600$. (b) Boundary conditions such that the mean pressure gradient is time independent. The notation is the same as in (a) with the addition that short dashed lines denotes steady waves with two positive eigenvalues and circles denote the branch of modulated waves which bifurcates from the steady waves. Solid circles denote stable modulated waves; open circles denote unstable modulated waves. The norm of the modulated waves is, in general, time dependent, and the two sets of circles are used to represent the extremes of the norm. The Reynolds number of the steady-wave limit point is $\mathrm{Re}_Q \simeq 3000$; the Reynolds numbers of the other bifurcations are not known precisely (see text). The arrows along the steady-wave branches indicate parametrized paths treated in Fig. 3.

pressure-gradient boundary conditions.[11] We argue that in the two-parameter space, (Re,μ), there is a codimension-two bifurcation that provides the basis for a comprehensive understanding of the dynamics near the limit point. This method of introducing a second parameter to bring together different phenomena into a unifying scenario is one of the most common and fruitful methods in bifurcation analysis.[12] With the parameter μ there are actually three parameters that can be considered, namely, Re, μ, and wavelength L. While we restrict our attention to flows that are periodic in the streamwise direction, we shall not investigate the wavelength parameter explicitly. Our results should apply to a large range of wavelengths.

As we shall show, the 2-D stability problem of steady waves near the limit point provides a rare opportunity to apply bifurcation theory to finite-amplitude solutions of the Navier–Stokes equations for which analytic expressions are not available. Based only on the numerical studies at constant flux and constant mean pressure gradient, we shall be able to piece together a complete picture for the stability of steady waves near the limit point and for the dynamics of the modulated waves. In so doing, *we shall make specific predictions about finite-amplitude solutions to the Navier–Stokes equations.*

We note at the outset that we shall not strive at mathematical rigor; instead we shall focus on understanding the various bifurcations involved in the problem. We work under the supposition that the simplest explanation consistent with bifurcation theory is correct.[13] We rely on assumptions that are probably true, yet extremely difficult to verify directly. We make no attempt to verify these assumptions and instead leave the ultimate test of our results to future numerical studies of the Navier–Stokes equations.

II. PRELIMINARIES

A. Boundary conditions and Reynolds numbers

While we shall not analyze the Navier–Stokes equations directly, we do wish to give a precise meaning to the parameter μ in terms of boundary conditions for the Navier–Stokes equations. In addition, we comment on the variety of Reynolds numbers that it is possible to define in plane Poiseuille flow.

Consider the 2-D Navier–Stokes equations written in the streamfunction formulation

$$\frac{\partial \nabla^2 \tilde{\Psi}}{\partial t} + \tilde{\Psi}_y \nabla^2 \tilde{\Psi}_x - \tilde{\Psi}_x \nabla^2 \tilde{\Psi}_y = \nu \nabla^4 \tilde{\Psi},$$

where ν is the kinematic viscosity. Tildes denote dimensional quantities and subscripts denote differentiation. The 2-D velocity field is given by $\mathbf{u}(x,y) = \nabla \tilde{\Psi} \times \hat{\mathbf{z}}$.

We confine our considerations to flows which are periodic in the streamwise direction x with wavelength L. That is, we assume

$$\tilde{\Psi}(x,y,t) = \tilde{\Psi}(x+L,y,t).$$

We decompose the streamfunction as $\tilde{\Psi}(x,y,t) = \tilde{\Psi}_p + \tilde{\psi}(x,y,t)$, where $\tilde{\Psi}_p = U_0(y - y^3/3h^2)$ is the streamfunction for the parabolic velocity profile with centerline velocity U_0, and $\tilde{\psi}$ is a perturbation of this profile. At present, U_0 is unspecified. Nondimensionalizing by the channel half-width h and the velocity U_0, we obtain

$$\frac{\partial \nabla^2 \psi}{\partial t} + (\psi_y + 1 - y^2)\nabla^2 \psi_x - \psi_x(\nabla^2 \psi_y - 2) = \frac{1}{\mathrm{Re}} \nabla^4 \psi, \tag{1}$$

where $\mathrm{Re} \equiv hU_0/\nu$.

In terms of the streamfunction, no-slip boundary conditions at the walls are

$$\psi_x(x,-1,t) = 0, \tag{2}$$

$$\psi_x(x,1,t) = 0, \tag{3}$$

and

$$\psi_y(x,-1,t) = 0, \tag{4}$$

$$\psi_y(x,1,t) = 0. \tag{5}$$

These boundary conditions are not, however, sufficient to determine ψ because (2) and (3) leave an arbitrariness in the value of ψ at $y = \pm 1$.

We are free to add an arbitrary constant to ψ, and we use this freedom to fix the value of ψ at $y = -1$. Thus we replace (2) with the boundary condition

$$\psi(x,-1,t)=0. \tag{6}$$

There is still an arbitrariness in ψ at $y=+1$, and the specification of ψ here depends on the physical situation we wish to describe.

Consider first the physical situation in which the flux Q is prescribed for the flow. In terms of the streamfunction, the flux Q is

$$Q=[\,\tilde{\Psi}\,]^{h}_{-h}=[\,\tilde{\Psi}_p+\tilde{\psi}\,]^{h}_{-h}=\tfrac{4}{3}U_0h+[\,\tilde{\psi}\,]^{h}_{-h}. \tag{7}$$

Under these circumstances it is convenient to let $U_0=3Q/4h$. Then (7) becomes

$$[\,\tilde{\psi}\,]^{h}_{-h}=0.$$

Nondimensionalizing and using (6), we obtain for the boundary conditions on ψ at $y=+1$,

$$\psi(x,1,t)=0. \tag{8}$$

Equations (4)–(6) and (8) constitute a complete set of boundary conditions for the Navier–Stokes equations (1). The Reynolds number is expressed in terms of the flux as

$$\mathrm{Re}_Q=hU_0/\nu=3Q/4\nu,$$

where the subscript Q emphasizes that this expression for the Reynolds number is appropriate for flows with time-independent flux.

The situation is as follows: the velocity U_0 in the definition of Reynolds number needs to be specified. In an experiment in which the flux Q is held constant, a natural choice for this velocity is the centerline velocity of the parabolic profile with flux Q. We then view the fluid flow as the sum of a parabolic profile (given by $\tilde{\Psi}_p$) with flux Q, plus a perturbation (given by $\tilde{\psi}$) that makes no contribution to the flux.

Consider now the physical situation in which the total pressure drop over the streamwise length of a real channel is maintained constant. Under our assumption of periodicity in the streamwise direction, this is modeled by a constant pressure drop across the period length L. Because the change in pressure, Δp, over length L and the mean pressure gradient P are simply related by

$$P=\frac{\Delta p}{L}=\frac{1}{L}\int_x^{x+L}\frac{\partial p}{\partial x'}\,dx',$$

we consider boundary conditions appropriate for the case in which the mean pressure gradient is constant. A straightforward calculation[4] gives the mean pressure gradient in terms of the streamfunction as

$$P=-\frac{1}{2h}[\,\bar{\tilde{\Psi}}_t\,]^{h}_{-h}+\frac{\nu}{2h}[\,\bar{\tilde{\Psi}}_{yy}\,]^{h}_{-h},$$

$$=-\frac{1}{2h}[\,\bar{\tilde{\psi}}_t\,]^{h}_{-h}-\frac{2\nu U_0}{h^2}+\frac{\nu}{2h}[\,\bar{\tilde{\psi}}_{yy}\,]^{h}_{-h}, \tag{9}$$

where bars denote averages over length L. Setting $U_0=-h^2P/2\nu$, Eq. (9) becomes

$$-(1/2h)[\,\bar{\tilde{\psi}}_t\,]^{h}_{-h}+(\nu/2h)[\,\bar{\tilde{\psi}}_{yy}\,]^{h}_{-h}=0.$$

Nondimensionalizing and using (6) this becomes

$$\mathrm{Re}\,\psi_t(x,1,t)-[\,\bar{\psi}_{yy}\,]^{1}_{-1}=0. \tag{10}$$

Note that $\bar{\psi}_t=\psi_t$ at $y=+1$. In this case the Reynolds number is expressed in terms of the mean pressure gradient as

$$\mathrm{Re}_P=hU_0/\nu=-h^3P/2\nu^2,$$

where the subscript emphasizes that this expression for the Reynolds number corresponds to the case of time-independent mean pressure gradient.

Equations (4)–(6) and (10) also constitute a complete set of boundary conditions for the Navier–Stokes equations (1), and are appropriate when the mean pressure gradient is fixed for the flow. The interpretation of the Reynolds number is much the same as in the case of fixed flux. In an experiment in which the mean pressure gradient P is constant, we chose U_0 to be the centerline velocity of the parabolic profile with pressure gradient P. Boundary condition (10) ensures that the perturbation ψ makes no contribution to the mean pressure gradient.

We now interpolate between the above two cases. To do this we derive appropriate boundary conditions for a hypothetical experiment in which a linear combination of the flux and the mean pressure gradient is maintained constant. That is, we suppose an experimental apparatus such that

$$aQ+bP=\text{const}, \tag{11}$$

where a and b are dimensional constants reflecting the trade off between flux and pressure gradient in the apparatus. (The nondimensionalized ratio of a to b is ultimately the important quantity.) The value of the "constant" determines the Reynolds number and is presumably under experimental control.

From the preceding analysis, the left-hand side of Eq. (11) can be evaluated in terms of the streamfunction as

$$\begin{aligned} aQ+bP&=a[\,\tilde{\Psi}\,]^{h}_{-h}-\frac{b}{2h}[\,\bar{\tilde{\Psi}}_t\,]^{h}_{-h}+\frac{b\nu}{2h}[\,\bar{\tilde{\Psi}}_{yy}\,]^{h}_{-h}\\ &=a\left(\frac{4}{3}U_0h\right)+b\left(\frac{-2\nu U_0}{h^2}\right)+a[\,\tilde{\psi}\,]^{h}_{-h}\\ &\quad-\frac{b}{2h}[\,\bar{\tilde{\psi}}_t\,]^{h}_{-h}+\frac{b\nu}{2h}[\,\bar{\tilde{\psi}}_{yy}\,]^{h}_{-h}. \end{aligned} \tag{12}$$

If we let U_0 be given by

$$U_0=(aQ+bP)[\tfrac{4}{3}ah+(-2b\nu/h^2)\,]^{-1},$$

then (12) becomes

$$a[\,\tilde{\psi}\,]^{h}_{-h}-\frac{b}{2h}[\,\bar{\tilde{\psi}}_t\,]^{h}_{-h}+\frac{b\nu}{2h}[\,\bar{\tilde{\psi}}_{yy}\,]^{h}_{-h}=0.$$

Nondimensionlizing, using Eq. (6), and letting

$$\mu=-(2h^3/3\nu)(a/b)$$

be the appropriate nondimensionalized ratio of a and b, we obtain for the last boundary condition on ψ,

$$3\mu\psi(x,1,t) + \mathrm{Re}\,\psi_t(x,1,t) - [\bar{\psi}_{yy}]_{-1}^{1} = 0, \tag{13}$$

The Reynolds number is given by

$$\mathrm{Re} = \frac{hU_0}{\nu} = \left(\mu\frac{3Q}{4\nu} - \frac{h^3P}{2\nu^2}\right)(\mu+1)^{-1}$$

$$= \frac{\mu\,\mathrm{Re}_Q + \mathrm{Re}_P}{\mu+1}. \tag{14}$$

Equation (13) is the desired boundary condition expressed in terms of the dimensionless parameter μ; $\mu = 0$ corresponds to constant mean pressure gradient and $\mu = \infty$ corresponds to constant flux. Note that the factor of 3 cannot be eliminated from (13) without it appearing in (14). We feel that it more naturally belongs in (13).

The interpretation of the Reynolds number in (14) is as follows. Consider an experiment with specific values of a, b (having nondimensionalized ratio μ), and some specified value of the constant on the right-hand side of (11). To define a Reynolds number, we need to specify a value for U_0, and to be consistent with the definition of Reynolds number in the limiting cases $\mu = 0$ and $\mu = \infty$, we take U_0 to be the centerline velocity of the parabolic profile $\tilde{\Psi}_p$, whose flux and pressure gradient satisfy (11). We view the flow field as the sum of this parabolic profile, plus a perturbation ψ, whose flux and mean pressure gradient satisfy $aQ + bP = 0$, i.e., Eq. (13).

As has been noted previously,[3,4,14–16] there is an arbitrariness in the definition of Reynolds numbers for Poiseuille flow. For example, in the case of steady waves, i.e., $\psi(x,y,t) = \psi(x - ct,y,0)$, both the flux and the mean pressure gradient are constant, that is, if a steady wave satisfies (8), then it also satisfies (10). Hence, in the case of steady waves, there is equal justification for basing the Reynolds number on the flux as on the mean pressure gradient. However, $\mathrm{Re}_Q \neq \mathrm{Re}_P$, and in general $\mathrm{Re}_Q < \mathrm{Re}_P$ (see Refs. 14–16). The reason is that the centerline velocity of the parabolic profile having the flux of a steady wave does not equal the centerline velocity of the parabolic profile having the mean pressure gradient of the steady wave: the value of U_0 in the definition of Reynolds number depends on how one (arbitrarily) chooses to view the flow. Moreover, steady waves satisfy (13) for all values of μ. Thus to a given steady wave, one can assign any of an infinity of values to the Reynolds number depending on how one chooses to view the flow, that is, depending on what value of μ one chooses as a basis for defining the Reynolds number. In fact, by considering constraints other than (11), e.g., nonlinear combinations of flux and pressure, it is possible to define still more Reynolds numbers. We suggest that, in general, the Reynolds number be based on either the instantaneous or the time-averaged flux, for the flux is experimentally the most accessible quantity.

In this paper we shall take the point of view that is theoretically the simplest: Eqs. (4)–(6) and (13) constitute a complete set of boundary conditions for the Navier–Stokes equations (1). Together, (1) and its boundary conditions contain two parameters, Re and μ, and we seek to understand the solutions to (1) as a function of these two parameters. We stress that in the two-parameter space (Re,μ) there is no ambiguity in the meaning of Reynolds number; at each value of μ, the Reynolds number has a precise interpretation via (14).

B. Reduction to amplitude equations

In this section we discuss the relationship between the Navier–Stokes equations (1) and the amplitude equations, or normal forms, which we analyze in later sections. We relegate most of the details to Appendix B. While the reduction to amplitude equations is, in principle, straightforward, we are interested here in *finite-amplitude* waves and not small perturbations of the parabolic profile. Therefore we must expand about a nontrivial, finite-amplitude solution for which we do not have an analytic expression. Because of this, an analytic reduction of the Navier–Stokes equations to a set of amplitude equations is not possible. Nevertheless, from the numerical studies of Pugh and Saffman[3] and Soibelman,[4] and from some genericity assumptions, it is possible to determine the form of the amplitude equations.

We first discuss the translational symmetry of the channel, as this has important consequences for the amplitude equations that we consider. Because we restrict our considerations to solutions periodic in the streamwise direction x, the translational symmetry of the channel becomes the symmetry of the circle [specifically, the group of orientation preserving rotations in the plane: SO (2)]. The implications of this symmetry group in bifurcation has been discussed at length.[17–19] Under the assumption of periodicity, the coordinate x can be replaced by a periodic coordinate θ, and the steady waves in Poiseuille flow are formally rotating waves, directly analogous to those in the Couette–Taylor problem. We return to this point in Sec. V.

Steady waves obey the condition $\psi(x,y,t) = \psi(x - ct,y,0)$, where c is the wave speed. Thus by making the boost, $x' = x - ct$, from laboratory-fixed coordinates to coordinates moving with wave speed c, steady waves are seen as time independent. Similarly, in an appropriate frame of reference, the modulated waves are periodic in time. These facts derive directly from the symmetry of the problem.[17,18]

Thus, in our analysis, we wish to treat the steady waves as steady states and the modulated waves as periodic orbits; however, there are two problems with this. First, the steady states and periodic orbits obtained making the appropriate boosts are not isolated because there is an arbitrariness in the phase of the waves. Second, and more importantly, we are interested in cases in which, at given parameter values, there exists more than one steady-wave solution and possibly a modulated-wave solution to the Navier–Stokes equations. In general, these solutions will have different wave speeds, so that there does not exist a frame of reference in which all states simultaneously take on their "simplified form." There is a way around this problem which is briefly outlined in Appendix B. In essence, by considering the dynamics on a Poincaré section, we are able to eliminate simultaneously the wave speed of all waves from the dynamics.

After eliminating the wave speed, the next step in the reduction to amplitude equations consists of arguing that there are only two active modes near the Reynolds number limit point and that all other modes are slaved to these two. This is well justified based on the numerically obtained eigenvalues as discussed in the next section. Thus from the symmetry of the problem, and from the number of eigenvalues near zero, we argue that the dynamics near the Reynolds number limit point, can be captured with a pair of amplitude equations:

$$\dot{A}_1 = F_1(A_1, A_2), \qquad \dot{A}_2 = F_2(A_1, A_2), \tag{15}$$

where A_1 and A_2 are real amplitudes, which, in principle, are related to the streamfunction of the Navier–Stokes equations. In terms of these amplitude equations, steady waves are represented as steady states and modulated waves are represented as periodic orbits.

The remaining step in determining the amplitude equations consists of finding the simplest expansion for F_1 and F_2 that is consistent with the numerical results of Pugh and Saffman[3] and Soibelman.[4] This is the subject of the next section.

III. DOUBLE-ZERO BIFURCATION

A. Eigenvalues

The codimension-two bifurcation central to our analysis is the double-zero (DZ) bifurcation. This bifurcation is defined by the condition that the linearized equations have a zero eigenvalue with algebraic multiplicity 2 and geometric multiplicity 1. That is, after an appropriate similarity transformation, the linearization contains the Jordan block

$$\begin{bmatrix} 0 & 1 \\ 0 & 0 \end{bmatrix}. \tag{16}$$

This codimension-two bifurcation has been studied and completely classified by Takens,[20] and Bogdanov.[21,22] A pedagogical treatment can be found in Refs. 23 and 24.

The principal observation on which our analysis rests is that the steady waves must have a double-zero eigenvalue at some value of μ between zero and infinity.[25] This can be deduced immediately from eigenvalue spectra at $\mu = 0$ and $\mu = \infty$, and from continuity of the eigenvalues. At $\mu = \infty$ the eigenvalue spectrum at the limit point in Reynolds number is as shown in Fig. 2(a). There is a zero eigenvalue (as there must be at a limit point) and all the other eigenvalues are negative. The eigenvalue spectrum at the limit point when $\mu = 0$ is shown in Fig. 2(c). Here, there is one positive eigenvalue, again a zero eigenvalue, and all other eigenvalues are negative. If we vary μ from 0 to ∞ while adjusting Re so as to remain at the limit point, i.e., so as to maintain a zero eigenvalue, then by continuity, at some value of μ the positive eigenvalue in Fig. 2(c) must cross zero. Therefore at some value of Re and μ there must be a double-zero eigenvalue as illustrated in Fig. 2(b). Generically,[26] the linearization at this point will contain a

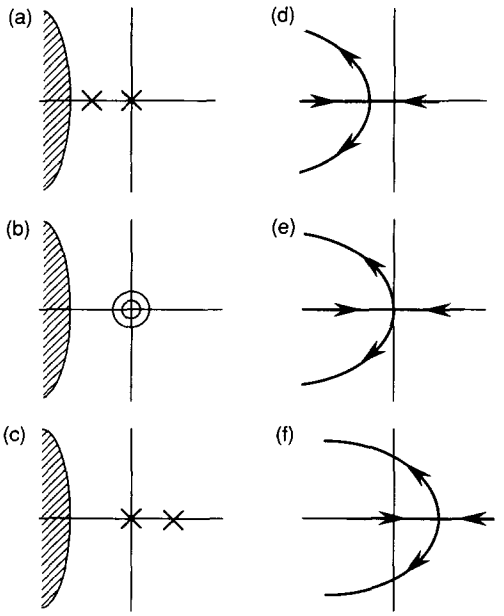

FIG. 2. (a)–(c) Location, in the complex plane, of the eigenvalues for the steady waves. There are only two relevant eigenvalues, all others are bounded away from zero as indicated by the shaded region in each plot. (a) Eigenvalues for the steady waves at the limit point in Reynolds number in the case of constant-flux boundary conditions, $\mu = \infty$. (b) Double-zero eigenvalue, indicated by the concentric circles at the origin, at the intermediate boundary condition, $\mu = \mu_c$. (c) Eigenvalues for the steady waves at the limit point in Reynolds number in the case of constant-mean-pressure-gradient boundary conditions, $\mu = 0$. (d)–(f) Paths of the two relevant eigenvalues in (a)–(c), respectively, as functions of arclength along paths illustrated in Fig. 1.

Jordan block of the form (16). We label the parameter values of the DZ by μ_c and Re_c, and the streamfunction with the double-zero eigenvalue by ψ_c. [Strictly speaking, ψ_c is the streamfunction with the double zero eigenvalues such that $\psi_c(x = 0, y = 0) = K$, as discussed in Appendix B.]

Much of the behavior near the limit point can be inferred immediately from the eigenvalues shown in Figs. 2(a)–2(c) without resorting to normal-form calculations. In particular, the bifurcation to a modulated wave can be deduced directly. To see this, it is best to consider the behavior of the two relevant eigenvalues as one moves along the branch of steady waves from the lower branch, around the nose, and onto the upper branch. That is, we consider paths along the steady-wave branch, like those illustrated in Fig. 1, and examine the corresponding paths of eigenvalues in the complex plane. Figures 2(d)–2(f) show the behavior of the two relevant eigenvalues for three values of μ.

Consider first Fig. 2(e), which corresponds to $\mu = \mu_c$. Starting on the lower branch there is one positive and one negative eigenvalue. As one approaches the limit point, the two eigenvalues approach zero from above and below, and they collide in a DZ at the limit point. Generically, when two eigenvalues (of a real system) collide on the real axis as a parameter is varied, they will move off the real axis in a locally parabolic path as illustrated in Fig. 2(e). This is easily seen by examining the general quadratic equation

with real coefficients. We assume a left-opening parabola because Pugh and Saffman[3] and Soibelman[4,27] find a left-opening parabola at $\mu = 0$ and $\mu = \infty$. In addition, the simplest scenario obtains when the parabola opens to the left. The direction of the eigenvalue path is an important feature which we return to later.

The behavior of the eigenvalues for μ near μ_c is found by considering perturbations to the behavior at $\mu = \mu_c$. We know that the two eigenvalues will collide on the real axis, but away from zero, for μ near μ_c. For example, with $\mu > \mu_c$, as in Fig. 2(d), the eigenvalues collide on the negative real axis. Thus the following occurs as we move along the steady-wave branch: the positive eigenvalue crosses zero at the limit point, and, hence, on the upper branch both eigenvalues have negative real part. At some point on the upper branch we expect the eigenvalues to collide and become complex. The numerical studies of Soibelman[27] reveal that this indeed occurs when $\mu = \infty$.

The case of $\mu < \mu_c$ [Fig. 2(f)] is more important. At the limit point, the negative eigenvalue crosses zero giving two positive eigenvalues on the upper branch. The two eigenvalues collide and become a complex-conjugate pair. Then, because the parabola in Fig. 2(e) opens to the left, it must do for μ sufficiently near μ_c. Thus the eigenvalues must cross the imaginary axis as a complex-conjugate pair. At this point the upper branch becomes stable via a Hopf bifurcation and modulated waves bifurcate from the upper branch.

Thus knowing the eigenvalue spectra in Figs. 2(a) and 2(c) we are able to deduce the DZ in Fig. 2(b). From this we know that an eigenvalue path like that of Fig. 2(e) must exist, and thus that modulated waves must bifurcate from the steady waves. Even if the parabola in Figs. 2(e) opened to the right, modulated waves would still exist, except for $\mu > \mu_c$. Because, we already knew of the modulated waves from the numerical studies of Pugh and Saffman and Soibelman, we seek stronger conclusions from our analysis. For this we turn to the normal-form equations for the DZ.

B. Normal-form equations: Second order

In this subsection and the next, we examine the normal form equations for the DZ. The essential idea here is the following. We expand the amplitude equations (15) in a finite Taylor series, and then use transformations of the amplitudes A_1 and A_2 to eliminate all "nonessential" terms from the series. By definition, the normal forms contain only those "essential" terms that cannot be removed by coordinate transformation.[23,24] In this section we consider the normal form equations with terms up to second order, and in the next subsection, we include terms up to third order.

There are two reasons why we are able to proceed in this way for the channel problem: first, the essential terms appearing in the normal-form equations are determined from the linearization only, and we know the linearization—it is Jordan block (16). Second, the normal-form equations for the DZ are very simple and there is enough information available from the numerical studies of Pugh and Saffman and Soibelman for us to evaluate, at least qualitatively, the coefficients in the expansion. Thus, even without explicit formulas relating the amplitudes A_1 and A_2 in the normal-form equations to the steamfunction ψ in the Navier–Stokes equations, we are able to derive the evolution equations for A_1 and A_2. From these evolution equations we are able to gain an understanding of the solutions of the Navier–Stokes equations.

The general second-order expansion of the amplitude equations is

$$\dot{A}_1 = F_1(A_1,A_2) = k_{11}A_1 + k_{12}A_2 + k_{13}A_1^2 + k_{14}A_1A_2 + k_{15}A_2^2,$$

$$\dot{A}_2 = F_2(A_1,A_2) = k_{21}A_1 + k_{22}A_2 + k_{23}A_1^2 + k_{24}A_1A_2 + k_{25}A_2^2.$$

At the double zero, k_{11}, k_{21}, and k_{22} must be zero, i.e., the linearization of the amplitude equations must be in Jordan form (16). Momentarily we will scale $k_{12} = 1$. In addition, it is straightforward to show[23] that there is a transformation,

$$A_1 = g_1(A_1',A_2'),\ A_2 = g_2(A_1',A_2'),$$

which preserves the form of the linear terms, but which make all but two of the second-order coefficients zero. Making this transformation, the only terms appearing in the normal-form equations for the DZ are

$$\begin{aligned} \dot{A}_1' &= k_{12}A_2', \\ \dot{A}_2' &= k_{23}A_1'^2 + k_{24}A_1'A_2', \end{aligned} \tag{17}$$

where generically k_{12}, k_{23}, and k_{24} are nonzero.

By rescaling A_1', A_2', and time, we can set $k_{12} = 1$, $k_{23} = 1$, and $|k_{24}| = 1$. We cannot rescale k_{24} to $+1$, in general, without changing the sign of time, and we do not allow this because then the stability of states in the normal form will be different from the stability of states in the Navier– Stokes equations. Instead we determine the sign of k_{24} by comparing the stability of steady states in the normal form with the stability of the steady waves in the Navier–Stokes equations. Note that there is only one *bit* of information to be determined in (17): the sign of k_{24}.

Before proceeding, we must incorporate the parameter dependence into the normal form. Equations (17) describe the evolution of the amplitudes at the double zero only, i.e., for $\mathrm{Re} = \mathrm{Re}_c$ and $\mu = \mu_c$. It is, however, possible to "unfold" the normal form and find evolution equations that describe the dynamics at parameter values in the vicinity of the double-zero bifurcation. The procedure is much the same as that for obtaining (17), except that parameters are included in the series expansion. However, there are subtleties involved when parameters are included. For the double-zero eigenvalue, expensions have been obtained by Takens and Bogdanov so we simply give the result and refer the reader to Refs. 23, 24, and 21. The unfolded normal form is

$$\begin{aligned} \dot{A}_1 &= A_2, \\ \dot{A}_2 &= -\lambda_1 - \lambda_2 A_2 + A_1^2 + k_1 A_1 A_2, \end{aligned} \tag{18}$$

where we have dropped the primes and written k_1 for k_{24}. The unfolding parameters are λ_1 and λ_2. These must be functions of $\mathrm{Re}-\mathrm{Re}_c$ and $\mu-\mu_c$, though as in the case with the amplitudes, we do not have explicit formulas relating λ_1 and λ_2 to Re and μ. However, we expect λ_1 to be approximately proportional to $\mathrm{Re}-\mathrm{Re}_c$ and λ_2 to be approximately proportional to $\mu-\mu_c$.

We can now determine the sign of k_1. The steady states of (18) are given by

$$(A_1,A_2)=(\pm\sqrt{\lambda_1},0).$$

Thus there are two steady states for $\lambda_1>0$ and these steady states coalesce at $\lambda_1=0$. These steady states correspond to the steady wave on the upper and lower branches in Fig. 1. To determine k_1, we must find the stability of the steady states in the normal form. The stability of the steady states is given by the eigenvalues of the matrix

$$\begin{bmatrix} 0 & 1 \\ 2A_\pm & -\lambda_2+k_1A_\pm \end{bmatrix}, \tag{19}$$

where $A_\pm\equiv\pm\sqrt{\lambda_1}$.

Consider first the case $k_1=+1$. If $\lambda_1\gg|\lambda_2|$, corresponding to moderate Reynolds numbers, then the steady state $(A_-,0)$ has two negative eigenvalues and hence is stable. This steady state thus corresponds to the steady waves on the upper branch in Fig. 1. [In both cases, Figs. 1(a) and 1(b), the upper branch is stable at large enough Reynolds numbers.] The steady state $(A_+,0)$ has one positive eigenvalue and is a saddle. This steady state thus corresponds to the steady waves on the lower branch. For the case $k_1=-1$, the stability of the steady states in the normal form can be found simply by reversing the sign of time. In this case neither steady state is stable for λ_1 large. Thus only for $k_1=+1$ is the normal form compatible with the stability of the steady waves in the Navier–Stokes equations. With $k_1=+1$ the second-order normal form is completely determined.

We can now examine the behavior near the double zero based on the normal form. Figure 3 summarizes the situation and this is discussed at length elsewhere.[21,23,24] The limit point, or saddle-node, bifurcations occur when the linearization (19) has a zero eigenvalue. By inspection, (19) has a zero eigenvalue when $A_\pm=0$, i.e., when $\lambda_1=0$. Strictly speaking, we should exclude $\lambda_2=0$ from the set of saddle-node bifurcations, because $\lambda_1=\lambda_2=0$ gives the double-zero eigenvalue.

The locus of Hopf bifurcations is equally easy to find from the linearization (19). A complex-conjugate pair of the eigenvalue with zero real part occurs when

$$\lambda_2=-\sqrt{\lambda_1},\quad \lambda_1>0.$$

Thus Hopf bifurcations occur on a half-parabola terminating at the DZ. The frequency of the Hopf bifurcation is the imaginary part of the eigenvalue at the bifurcation: $\omega=\sqrt{-2\lambda_2}$. The DZ can be viewed as the collision between Hopf and saddle-node bifurcations in which the frequency of the Hopf bifurcation goes to zero.

In addition to the Hopf and saddle-node bifurcations, homoclinic orbits (saddle-loop bifurcations) are found

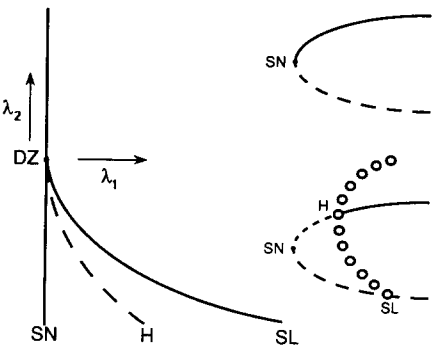

FIG. 3. Phase diagram and representative bifurcation diagrams for the second-order double-zero normal form. DZ denotes double zero, SN denotes saddle-node bifurcations (i.e., limit points), H denotes Hopf bifurcations, and SL denotes saddle-loop bifurcations. The bifurcation diagrams are functions of λ_1 at fixed values of λ_2 above and below the DZ. The notation for states is the same as in Fig. 1. The locus of Hopf bifurcations in the phase diagram is dashed to indicate that the Hopf bifurcations are subcritical.

near the DZ. Saddle-loop (SL) bifurcations can be thought of as a collision, in phase space, between a periodic orbit and a fixed point of the saddle type. [See Fig. 6(a) discussed in Sec. V.] At the SL bifurcation, the amplitude of the periodic orbit remains finite, while the period goes to infinity. The SL bifurcation has the effect of destroying (or creating, depending on the point of view) a periodic orbit. Nothing in particular happens to the fixed point itself. Thus the SL is a global bifurcation and no local analysis of the steady states, except very near the DZ, can detect it.

The locus of saddle loops approaches the DZ approximately parabolically. For a given value of λ_2, the λ_1 distance between the saddle-loop and the Hopf bifurcations is approximately the same as the λ_1 distance between the Hopf and saddle-node bifurcations. The periodic orbits are found only in the wedge between the loci of Hopf and saddle-loop bifurcations.

Turning then to the implications for the steady waves in channel flow, we find that, at least local to the DZ, the Hopf bifurcation on the upper branch approaches the limit point parabolically and disappears in a DZ bifurcation. The frequency of the Hopf bifurcation goes to zero at the DZ. Thus the period of the modulated waves, as see in the frame moving at the wave speed, goes to infinity. These facts can be deduced from the eigenvalues in Fig. 2. In addition, we expect that the modulated waves do not extend to very large Reynolds numbers, but terminate in a SL bifurcation by colliding with the lower branch of the steady waves. These are the first predictions from our analysis.

The reader should note that Fig. 3, and hence the second-order normal form (18), does not completely agree with the numerical computations of Soibelman shown in Fig. 1(b). Specifically, there is disagreement in the direction of the branch of modulated waves. For the numerical computations at constant mean pressure gradient, i.e., at $\mu=0$, the Hopf bifurcation computed by Soibelman is supercritical, yet in the normal form with $k_1=+1$, the Hopf bifurcation is always subcritical. (See Appendix A

for a brief discussion of the terminology for supercritical and subcritical.) While our analysis applies in the vicinity of the DZ, it does not apply for sufficiently negative λ_2, corresponding to μ near zero. To resolve this we must include higher-order terms in the normal-form expansion.

C. Normal-form equations: Third order

It is a simple matter to determine the essential terms in a third-order expansion of the double zero. There are only two third-order terms,[23] and the normal form is

$$\begin{aligned} \dot{A}_1 &= A_2, \\ \dot{A}_2 &= -\lambda_1 - \lambda_2 A_2 + A_1^2 + k_1 A_1 A_2 + k_2 A_1^3 - k_3 A_1^2 A_2, \end{aligned} \tag{20}$$

where k_1 is no longer taken to be of unit magnitude. Instead we chose a scaling such that $|k_3| = 1$. We shall see that k_3 plays much the same role in the third-order expansion as k_1 does in the second-order expansion. In fact, the minus sign preceding the $A_1^2 A_2$ term is added to make the signs of these coefficients correspond.

Considering k_1 as a parameter, normal form (20) can be viewed as an unfolding of the codimension-three bifurcation defined by the condition $\lambda_1 = \lambda_2 = k_1 = 0$. This codimension-three bifurcation is a double-zero eigenvalue with an additional degeneracy in the higher-order terms, i.e., $k_1 = 0$, such that the Hopf bifurcation is degenerate.[28] The theoretical treatment of this more degenerate bifurcation is not as complete as in the case of the simple double zero (18).

Rather than present in detail the dynamics of (20) as a function of three parameters, we shall view (20) as a set of model equations with two parameters λ_1 and λ_2, and three coefficients k_1, k_2, and k_3. We require k_1 to be sufficiently small that the third-order terms are important, that is, we are interested in small perturbations of the codimension-three point. The parameters in the normal form correspond to those of the problem at hand, namely, Re and μ; the three coefficients are to be determined by matching the dynamics of (20) to that found in the numerical results of Pugh and Saffman and Soibelman at $\mu = 0$ and $\mu = \infty$. Because k_3 is scaled to unit magnitude it can be determined exactly. While we are unable to determine quantitatively k_1 and k_2, we can determine the signs of these coefficients and this will be all that is needed to obtain a comprehensive picture of the dynamics near the Reynolds number limit point.

We first determine k_3, as we did in the previous section for k_1, by examining the stability of steady states. The steady states of (20) are given by

$$(A_1, A_2) = (A_{ss}, 0),$$

where A_{ss} is a solution to

$$0 = -\lambda_1 + A_{ss}^2 + k_2 A_{ss}^3. \tag{21}$$

When $\lambda_1 = 0$ this equation has a double root $A_{ss} = 0$. This is the limit point. The two steady states that are near zero for $\lambda_1 > 0$ are the only two steady states of interest; the third solution of (21) does not vanish at the multicritical point and therefore is not relevant. For $0 \leqslant \lambda_1 \ll 1/k_2^2$, the two relevant steady states are $A_{ss} \simeq \pm \sqrt{\lambda_1}$. Thus we shall label these two steady states by $A_\pm$ as before, but they are actually solutions to (21).

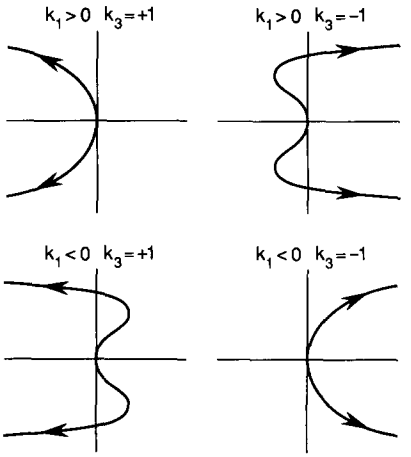

FIG. 4. The path, in the complex plane, of the two eigenvalues of steady state A_- for the third-order normal form, with different choices of k_1 and k_3. The paths are parametrized by λ_1 with the direction of increasing λ_1 as shown. For the cases shown, $\lambda_2 = 0$.

The stability of these steady states is given by the eigenvalues of the matrix

$$\begin{bmatrix} 0 & 1 \\ 2A_\pm + 3k_2 A_\pm^2 & -\lambda_2 + k_1 A_\pm - k_3 A_\pm^2 \end{bmatrix}. \tag{22}$$

The quickest way to determine the sign of k_3, is to consider the case $\lambda_2 = 0$. The eigenvalues for the two states A_+ and A_- are easily computed. One finds that for sufficiently small λ_1 (i.e., $0 < \lambda_1 \ll 1/k_2^2$), A_+ has one positive and one negative real eigenvalue; therefore A_+ is a saddle corresponding to the lower branch of steady waves in the channel flow problem (Fig. 1). The state A_- must therefore correspond to the upper branch of steady waves. The eigenvalues of A_- depend on the coefficients k_1 and k_3. Figure 4 shows the path of these eigenvalues in the complex plane as a function of λ_1 for different choices of k_1 and k_3. With the requirement that k_1 be sufficiently small so that the third-order terms are important, the stability of the steady state A_- is determined by the sign of k_3. At sufficiently large[29] λ_1, corresponding to sufficiently large Reynolds number, the state A_- has two eigenvalues with negative real part only if $k_3 = +1$. This also holds for $\lambda_2 \neq 0$. Thus we must take $k_3 = +1$ to have a stable steady state in the normal form corresponding to the stable upper branch of steady waves in Fig. 1.

We can now determine the sign of k_1 by comparing the eigenvalue paths for the normal form and with that of steady waves in the channel problem. We know from the numerical computations of Pugh and Saffman[3] and Soibelman[4,27] that at $\mu = 0$ and $\mu = \infty$ the path of eigenvalues is a left-opening parabola as shown in Figs. 2(d) and 2(f). It is thus reasonable to assume that this is also the case for all intermediate μ. As Fig. 4 shows, we must have $k_1 > 0$ in the normal form to have a left-opening parabola. Hence we require k_1 to be positive.

This leaves only k_2 to be determined. The sign of k_2 is found by matching the direction of the periodic-orbit branch in the normal form to the direction of the modulated wave branch found by Soibelman [Fig. 1(b)]. First, the steady state A_- of the normal form undergoes a Hopf bifurcation when

$$-\lambda_2 + k_1 A_- - k_3 A_-^2 = 0,$$
$$2A_- + 3k_2 A_-^2 < 0. \tag{23}$$

These conditions ensure that (22) has a complex-conjugate pair of eigenvalues with zero real part.

The direction of the periodic-orbit branch near the Hopf bifurcation is found in the following way: we take the bifurcation point given by (23), where A_- satisfies (21), and make a coordinate transformation which brings A_- to the origin. We then make a further transformation to express the amplitudes in polar form. At a Hopf bifurcation, the leading order terms in the evolution equations will be

$$\dot{A}_r = aA_r^3,$$
$$\dot{A}_\theta = \omega,$$

where A_r and A_θ are the amplitudes in polar form, $\omega^2 = -(2A_{-1} + 3k_2 A_{-1}^2)$ is the square of the imaginary part of the bifurcating eigenvalue, and a is the coefficient that determines whether the bifurcation is supercritical or subcritical: if $a>0$ the bifurcation is subcritical and the periodic orbit branch lies on the high-λ_1 side of the Hopf bifurcation. If $a<0$ the bifurcation is supercritical, and at least near the bifurcation, the periodic-orbit branch lies on the low-λ_1 side of the bifurcation (see Appendix A).

The computations are straightforward but lengthy, so we shall not reproduce them. The result is that we obtain an expression for a in terms of the coefficients of the normal form,

$$a = (1/8\omega^2)(k_1 + 3k_2\lambda_2). \tag{24}$$

We can now determine the sign of k_2. Soibelman has found that the Hopf bifurcation is supercritical at $\mu = 0$. Therefore we require the Hopf bifurcation in the normal form to be supercritical for sufficiently negative λ_2, corresponding to μ near zero. This means that a must be negative for sufficiently negative λ_2. The only way to achieve this is to require that k_2 be positive (note $k_1>0$). Thus the signs of all coefficients of the normal form are determined.

The situation is basically as follows. In the vicinity of a double-zero bifurcation with $k_1 \simeq 0$, there are a variety of possible scenarios depending on the coefficients k_1, k_2, and k_3 in the normal form. There is, however, only one scenario that is consistent with the following facts: (i) the upper branch of steady waves stabilizes at large enough Reynolds number, (ii) the path of eigenvalues is a left-opening parabola as in Fig. 2, and (iii) the Hopf bifurcation is supercritical at $\mu = 0$. This scenario, which obtains for $k_1>0$, $k_2>0$, and $k_3 = +1$, provides the simplest description of the steady and modulated waves which is consistent with bifurcation theory. We examine this scenario in the next section.

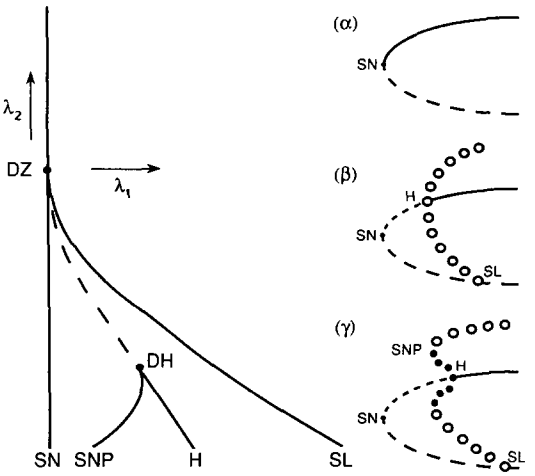

FIG. 5. Phase diagram and representative bifurcation diagrams for the third-order double-zero normal form. The notation is the same as in Figs. 1 and 4, with the following additions: DH denotes degenerate Hopf bifurcation and SNP denotes saddle-node-of-periodic-orbits bifurcation, i.e., the limit point of the periodic-orbit branch. In the phase diagram, supercritical and subcritical Hopf bifurcations are indicated with solid and dashed lines, respectively. The bifurcation diagrams are functions of λ_1 at three values of λ_2: (α), λ_2 above the DZ; (β), λ_2 between the DZ and the DH; (γ), λ_2 below the DH.

IV. RESULTS

Figure 5 summarizes our results, based on the third-order normal-form expansion, for the dynamics near the limit point in Reynolds number. We show both the two-parameter phase diagram (also called a bifurcation set) and representative bifurcation diagrams. The parameters shown are λ_1 and λ_2 of the normal-form equations, but we expect that λ_1 is approximately proportional to $\mathrm{Re} - \mathrm{Re}_c$, and that λ_2 is approximately proportional to $\mu - \mu_c$, where Re_c and μ_c are the parameter values of the DZ. Thus the phase diagram is essentially the two-parameter space (Re,μ) with Re the horizontal parameter and μ the vertical parameter. The bifurcation diagrams are slices through the phase diagram at three representative values of λ_2. These bifurcation diagrams are essentially Reynolds number bifurcation diagrams for three different boundary conditions.

We first describe the situation in detail and then recount exactly the predictions arrived at through our analysis. Consider first bifurcation diagram (γ), which corresponds to μ near zero, which in turn corresponds to constant-mean-pressure-gradient boundary conditions. Bifurcation diagram (γ) is essentially that of Fig. 1(b), except that in (γ) the branch of modulated waves terminates in a saddle-loop bifurcation by colliding with the lower branch of steady waves. Recall that the fate of the modulated waves in Fig. 1(b) was not determined by the numerical computations of Soibelman.

Consider next bifurcation diagram (β). This bifurcation diagram is a slice through the phase diagram at a value of μ above the degenerate Hopf (DH) bifurcation. The modulated-wave branch is born unstable in (β) and it terminates as before in a saddle-loop bifurcation with the

lower branch of steady waves. What has occurred in going from diagram (γ) to diagram (β) is that the Hopf bifurcation has changed from supercritical to subcritical, and consequently, there is no longer a limit point (SNP) for the modulated-wave branch. The DH bifurcation is discussed briefly in Appendix A. For the third-order normal form, the DH occurs when the right-hand side of Eq. (24) equals zero, that is, when $\lambda_2 = -k_1/3k_2$.

As one increases the parameter μ further, both the Hopf and saddle-loop bifurcations approach the limit point of the steady-wave branch and together disappear at the DZ bifurcation. For values of μ above the DZ the situation is as in bifurcation diagram (α), which is the same as Fig. 1(a). The steady-wave branch stabilizes at the limit point and there are no other bifurcations in the vicinity of the limit point.

Thus we have the desired comprehensive picture of the dynamics as a function of the two parameters Re and μ. We expect Fig. 5 to be in qualitative agreement with the phase diagram for the Navier–Stokes equations, although some quantitative variation is to be expected. For example, we know that the Reynolds number of the limit point varies slightly as a function of μ (see caption, Fig. 1), whereas the limit points in Fig. 5 occur at a fixed value of λ_1. Detailed, quantitative, predictions are simply beyond the scope of our treatment: we cannot predict the Reynolds number or boundary-condition parameter for any of the bifurcations, we can only predict their existence.

The predictions that we make, i.e., the features of Fig. 5 not contained in previous numerical computations, are the following.

(1) *Existence of the homoclinic orbit for the modulated waves.* This is perhaps the most important prediction because it applies at $\mu = 0$, i.e., constant mean pressure gradient, and this is one of the most frequently investigated boundary conditions for Poiseuille flow. There are two other predictions that are a direct result of the existence of the homoclinic orbit.

(a) At the saddle-loop bifurcation, the wave speed of the modulated wave must equal the wave speed of the steady wave on the lower branch. This is simply because, at the saddle-loop bifurcation, there is a reference frame in which simultaneously the modulated waves are seen as a closed orbit and the lower-branch steady wave is seen as a fixed point.

(b) The period of the modulated waves goes to infinity in a well-prescribed way. Namely, the period of the modulated waves T, as seen in the frame moving at the wave speed, goes as $T \sim -\log(\mathrm{Re}_{\mathrm{SL}} - \mathrm{Re})$, where $\mathrm{Re}_{\mathrm{SL}}$ is the Reynolds number of the saddle-loop bifurcation (see Ref. 23). This scaling law will be difficult to verify in practice because near the homoclinic orbit the modulated waves have a strong relaxational character. That is, in the moving frame, the modulated waves are seen as periodic orbits that spend a long time in a pseudosteady state (approximately the lower-branch steady wave) and then undergo a comparatively fast burst. Periodic states of this kind, i.e., very far from harmonic, require many modes if they are to be computed with a steady code of the kind used by Soibelman.

(2) *Existence of the degenerate Hopf bifurcation on the upper branch of steady waves.* This is an important result in that it is a statement about the *nonlinear* stability of finite-amplitude waves for boundary conditions that have not yet been investigated numerically. The existence of this DH bifurcation implies the disappearance of the limit point for the modulated-wave branch (SNP). There is a scaling law for the disappearance of the SNP, namely the locus of limit points meets the locus of Hopf bifurcations parabolically. This parabolic behavior is indicated in Fig. 5 (see also Appendix A).

(3) *Existence of the double-zero bifurcation itself.* At the double zero, the loci of Hopf and saddle-loop bifurcations terminate. The loci of both bifurcations approach the DZ parabolically. Moreover, near the DZ we expect that, in the Reynolds number bifurcation diagrams, the saddle-loop bifurcation will be approximately twice as far from the limit point, as measured in Reynolds number, as the Hopf bifurcation is from the limit point. Finally, the frequency of the Hopf bifurcation will go to zero as the DZ is approached.

V. DISCUSSION AND CONCLUSION

We have constructed a complete phase diagram from knowledge of the situation just at the extreme boundary conditions $\mu = 0$ and $\mu = \infty$. What has made this possible is the fact that all the dynamics near the limit point can be captured with just two amplitude equations, and in the corresponding two-dimensional phase space, the possible scenarios are greatly limited. Ultimately, the translational symmetry of the channel is responsible for allowing the dynamics to be captured in a two-dimensional phase space. Therefore we begin our discussion by noting the important implications of the channel's symmetry.

The modulated waves lie on a torus in the full phase space of the Navier–Stokes equations and, in general, it would not be possible to describe accurately the dynamics of these waves with only two (continuous-time) amplitude equations. In particular, the homoclinic orbits (saddle-loop bifurcations) which we have described would, in the absence of symmetry, imply the existence of complex dynamics, i.e., horseshoes.[23,24,30,31] Hence at least three amplitudes would, in general, be necessary to capture the dynamics in the vicinity of this bifurcation. However, it is straightforward to prove that, owing to the symmetry of the channel, if a point lies on both the stable and unstable manifold of the saddle (lower-branch steady wave), then the unstable manifold is contained within the stable manifold and complex dynamics does not occur. This is illustrated in Fig. 6(a) where we show the saddle-loop bifurcation in the case of symmetry. This homoclinic orbit can be captured by just two differential equations. It is for this reason that we expect the double-zero normal form to provide an accurate description of the dynamics near the Reynolds number limit point, and it is for this reason that

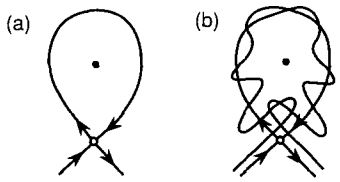

FIG. 6. (a) Saddle-loop bifurcation for channel flow in the case of translational symmetry. The saddle point (lower steady state) corresponds to the lower-branch steady wave; the upper steady state is stable and corresponds to the upper-branch steady wave. (b) Homoclinic orbit expected for channel flow in the case of broken translational symmetry. Complex dynamics occurs in (b) but not in (a).

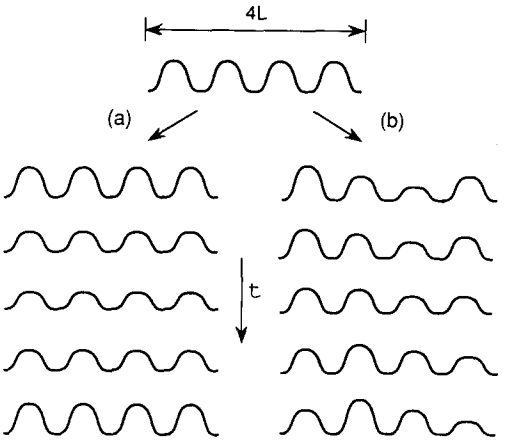

FIG. 7. Schematic representation of two possible bifurcations from steady (or rotating) waves to modulated waves. Four wavelengths of the bifurcating steady wave are shown at the top. The modulated waves are shown at five instants in time over one period. The representations are similar to those in Ref. 18, and correspond to observations in the reference frame moving at the wave speed. The modulated wave in (a) is superharmonic and has the same wavelength as the steady wave. The modulated wave in (b) is subharmonic and has four times the wavelength of the steady wave. Note that in a "box" of length $4L$, the steady wave has a fourfold symmetry. This symmetry is broken in (b) but not in (a).

continuous-time amplitude equations can provide a qualitatively exact interpolation of the Poincaré map in Appendix B. Simply put, because of the translational symmetry of the channel, the modulated waves behave as periodic orbits rather than as generic orbits on a torus. (This is a well-known result; e.g., Rand[18]).

An interesting situation arises if the translational symmetry of the channel is broken. Specifically, consider the case in which the translational symmetry is broken by a periodic perturbation with wavelength L in the streamwise direction. For small perturbation of this kind we can expect the homoclinic orbits to persist, but they will become transverse. This implies the existence of horseshoes and complex dynamics as illustrated in Fig. 6(b). Note that because trajectories cannot cross, this situation cannot be captured with a pair of continuous-time amplitude equations. Figure 6(b) must instead be viewed as a Poincaré section of fundamentally three-dimensional dynamics. (In the absence of symmetry, the Poincaré map of Appendix B cannot be exactly interpolated by a pair of differential equations.)

What is particularly interesting about periodic geometries is that such geometries have recently been considered by Karniadakis *et al.*[32] In these studies, geometry has been used as a "parameter" to unfold the subcritical nature of the primary instability occurring in Poiseuille flow. That is, Karniadakis *et al.* have found that in certain periodic channels, the primary instability is supercritical. This implies that for some value of the "geometric parameter" the primary instability is degenerate, i.e., on the borderline between subcritical and supercritical. It then would appear that by varying both the geometric parameter and the boundary-condition parameter μ presented here, it might be possible to bring together the bifurcation to modulated waves and the degenerate primary instability. We are not certain at this time whether such a situation is actually possible; however, if this situation does occur, then arbitrarily close to this bifurcation there will be transverse homoclinic orbits, i.e., *there will be complex dynamics arbitrarily close to the steady laminar state.*

There is a second aspect of the problem's symmetry worthy of note and this concerns the relationship of the steady and modulated waves studied here to the rotating and modulated waves found in the Couette–Taylor (CT) problem.[7] As noted at the outset, because we restrict our attention to solutions that are periodic in the streamwise direction x, steady waves in the channel are formally rotating waves as in the CT problem. The bifurcation from steady to modulated waves in Poiseuille flow is thus formally the same as the bifurcation to modulated waves in CT. The modulated waves studied here are, however, of a special type: they are superharmonic, that is, they are composed of the fundamental wavenumber and its harmonics. These waves have the same wavelength as the steady waves [see Fig. 7(a)]. Contrast these waves with the subharmonic modulated waves generally observed in the CT problem. Figure 7(b) shows a simple illustrative example; other examples can be found in Refs. 7 and 18. While modulated waves in Poiseuille flow will also be subharmonic in the general case, Pugh and Saffman and Soibelman considered only superharmonic bifurcations of steady waves, so that the only modulated waves they could possibly detect were superharmonic. From our analysis, however, we see that the particular modulated waves that bifurcate near the limit point issue from a double-zero bifurcation, and thus that they *must* be superharmonic. Basically, the reason is that the modulated waves arise from the interaction of two bifurcating eigenvalues. For each eigenvalue the corresponding steady-state bifurcation, i.e., the limit point above and below the DZ, is not subharmonic.[33] Hence we expect that under generic conditions the Hopf bifurcation arising from the interaction of these eigenvalues will likewise not be subharmonic. We do not offer a proof here and leave a more detailed discussion of this for future work.

The final point we make regarding the symmetry of the channel is that there is reflection symmetry (i.e., Z_2) in the spanwise coordinate y, which we have not yet addressed.

First note that the boundary conditions that we have derived for $\psi(x,y,t)$, specifically (6) and (13), are not, in general, reflection symmetric. However, this is simply a result of our choice for the overall (arbitrary) normalization of ψ. Renormalizing $\psi(x,y,t)$ by adding a function only of time, $K(t)$, the boundary conditions on ψ can be made reflection symmetric. It is clear that the velocity field satisfies symmetric boundary conditions.

We have ignored the reflection symmetry because it plays no significant role in the problem. The only way this symmetry might enter is that the steady waves might have so-called shift-and-reflect symmetry,[34] that is, the waves might be invariant under the transformation: evolve for time $T/2$, where T is the period in the laboratory frame, and reflect in y. The shift-and-reflect symmetry can only be of importance if this symmetry breaks in the vicinity of the double-zero bifurcation. The numerical computations of Pugh and Saffman and Soibelman would have detected this symmetry breaking if it existed, and yet it was not reported. Thus we are justified in ignoring the reflection symmetry in our analysis.

We turn now to a different issue. The computations of Pugh and Saffman[3] and Soibelman[4] were motivated by the desire to find nontrivial solutions of the Navier–Stokes equations at Reynolds numbers below that of the limit point for the steady-wave branch. The modulated waves detected by Pugh and Saffman were seen as a possible candidate for such solutions. While our analysis cannot completely rule out the possibility of the modulated waves extending below the steady-wave limit point, we can rule out any simple scenario. That is, if there are no other bifurcations of the modulated waves prior to the SNP (the limit point for the modulated-wave branch), then it is straightforward to show that the SNP must occur at a Reynolds number greater than that of the steady-wave limit point. That is, in Fig. 5, the locus of SNP's cannot cross the locus of SN's. The reason is that the modulated waves form a barrier which separates the upper and lower steady waves and prevents them from meeting at the limit point. Hence the modulated-wave branch must turn around prior to the two branches of steady waves meeting at the limit point. We stress that while this result is intimately related to the fact that the dynamics can be captured in a 2-D phase space, the argument can be formulated strictly in topological terms without assumptions regarding the dimensionality of the phase space in which the modulated and steady waves exist.[35] Therefore, while we know directly from the computations of Soibelman that the modulated waves do not extend below the steady-wave limit point, our analysis explains why this is to be expected. Moreover, our analysis shows that even at parameter values not considered by Soibelman, e.g., other wavelengths, the modulated waves bifurcating near the limit point are not good candidates for solutions extending to low Reynolds numbers.

Finally, we comment on the wavelength parameter L, which we have not included explicitly in our analysis. First, the (Re,μ) phase diagram in Fig. 5 is structurally stable and should hold for many values of L. In particular, Fig. 5 is based on numerical computations at $\alpha = 2\pi h/L = 1.1$, which is near the well-known "nose" of the neutral-stability surface in (Re,α,E) space as studied by Herbert.[6] Hence we expect Fig. 5 to hold for a range of values of L near the nose. Second, while for some values of L the phase diagram for the Navier–Stokes equations might not be that shown in Fig. 5, we anticipate that in many of these cases the phase diagram will be simple distortions of Fig. 5. In particular, we expect the location of the DZ and DH to be functions of L. For some values of L these bifurcations might move either all the way up to $\mu = \infty$ or all the way down to $\mu = 0$, in which case these bifurcations disappear from the phase diagram. We remark also that by varying all three parameters, Re, μ, and L, it might be possible to find the codimension-three point corresponding to $\lambda_1 = \lambda_2 = k_1 = 0$ in the third-order normal form. It would be quite interesting if such a point could be found.

In conclusion, we have proposed a comprehensive picture for the stability of the steady waves and for the dynamics of modulated waves near the Reynolds number limit point in 2-D plane Poiseuille flow. Through an analysis of the normal-form equations for the double-zero eigenvalue, we have arrived at the simplest description of the behavior near the limit point that is consistent both with the numerical computations of Pugh and Saffman[3] and Soibelman,[4] and with bifurcation theory. It is possible, however, that the simplest possibility does not obtain in practice and that a more complicated scenario holds. It is therefore important that our predictions be checked by numerical computations of the Navier–Stokes equations. We hope that such computations will be forthcoming.

ACKNOWLEDGMENTS

The author thanks I. Soibelman, P. G. Saffman, M. Schatz, L. S. Tuckerman, P. J. Holmes, and D. I. Meiron for helpful discussions.

This work has been supported by U. S. Department of Energy, Applied Mathematical Sciences, Grant No. DE-FG03-89ER25073, and by the Office of Naval Research, Grant No. N00014-85-K-0205 SRO.

APPENDIX A: DEGENERATE HOPF BIFURCATION

There is some variation in terminology for subcritical and supercritical bifurcations,[36] so in this appendix we describe briefly what is meant by these terms in this paper and in most of the dynamical systems literature.[8,21,23,36] We examine the degenerate, codimension-two situation at which a bifurcation changes from supercritical to subcritical.

Consider first the case for the Hopf bifurcation in the plane. In polar coordinates, the normal form is

$$\dot{r} = -\lambda r + ar^3,$$

$$\dot{\theta} = \omega + c\lambda + br^2.$$

The $\dot{r}$ equation does not contain θ, and can be considered separately. Bifurcation diagrams are shown in Fig. 8 for $a = \pm 1$. These may also be viewed as pitchfork bifurcations of equilibria; the terminology for supercritical and subcritical applies to such bifurcations as well.

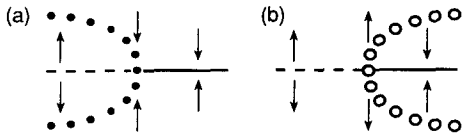

FIG. 8. Bifurcation diagrams for (a) supercritical Hopf bifurcation and (b) subcritical Hopf bifurcation. Arrows indicate the stability of the steady state $r=0$.

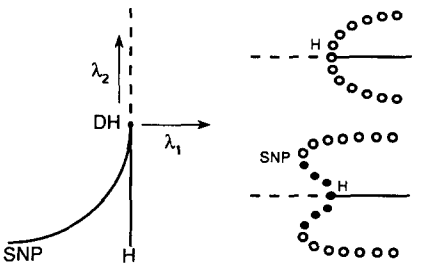

FIG. 9. Phase diagram and representative bifurcation diagrams for the degenerate-Hopf bifurcation. DH denotes the degenerate Hopf bifurcation, H denotes Hopf bifurcations, and SNP denotes saddle-node-of-periodic-orbits bifurcations. Supercritical and subcritical Hopf bifurcations are indicated with solid and dashed lines, respectively.

Everywhere except at the bifurcation point, the stability of the equilibrium $r=0$ is determined by linear analysis. At the bifurcation point, however, the stability of this equilibrium is determined by the higher-order terms, i.e., by the sign of a. *If the equilibrium is asymptotically stable at the bifurcation point, then the bifurcation is supercritical. If the equilibrium is asymptotically unstable at the bifurcation, that is, if the equilibrium is asymptotically stable after the transformation $t\to -t$, then the bifurcation is subcritical.* Note that at transcritical and saddle-node bifurcations, the equilibrium is neither asymptotically stable nor asymptotically unstable, and it makes no sense to speak of criticality (super or sub) for these bifurcations.

The following point is crucial: the criticality of a bifurcation is not determined by whether the bifurcating branches increase or decrease with the bifurcation parameter—the definition of criticality is independent of the problem parametrization.[37] The situation is directly analogous to that in equilibrium thermodynamics, where, for example, the order of a phase transition is independent of whether the temperature T or inverse temperature β is considered as the parameter. Subcritical bifurcations are analogous to first-order transitions and supercritical bifurcations to second-order transitions.

While the direction of the bifurcating branches is not determined in an absolute sense, the direction is determined with respect to the stability of the bifurcating equilibrium: if the bifurcation is supercritical, then the bifurcating solutions have the same stability as the original equilibrium and lie on the side of the bifurcation point corresponding to the positive eigenvalue. If the bifurcation is subcritical, then the opposite holds.

In higher-dimensional systems the criticality of a bifurcation is determined by the stability in the bifurcation direction only, i.e., by the stability along the center manifold only, and not by the overall stability of the bifurcating solutions. For example, in the three-dimensional system,

$$\dot r = -\lambda r + ar^3,$$

$$\dot\theta = \omega + c\lambda + br^2,$$

$$\dot z = z,$$

The criticality of the bifurcation at $\lambda = 0$ is determined from the r equation only, and while none of the solutions are stable due to instability in the z direction, the bifurcation is supercritical if $a<0$.

We now discuss the codimension-two bifurcation at which the criticality of the Hopf bifurcation changes. We refer to this bifurcation as the degenerate Hopf (DH) bifurcation. This bifurcation is important to the 2-D channel problem (Secs. III C and IV).

The $\dot r$ equations for the degenerate Hopf normal form is

$$\dot r = -\lambda_1 r + \lambda_2 r^3 + kr^5. \tag{A1}$$

The coefficient a in the Hopf normal form has been replaced by the parameter λ_2 and a fifth-order term has been added. As with the Hopf bifurcation, the essential behavior is contained solely in the $\dot r$ equation and we need not consider the $\dot\theta$ equation.

The phase diagram for $k>0$, which corresponds to the situation of interest in the channel problem, is shown in Fig. 9 . Hopf bifurcations occur at $\lambda_1 = 0$. They are subcritical if $\lambda_2>0$ and supercritical if $\lambda_2<0$. At $\lambda_2 = 0$ the bifurcation is, by the above definition, subcritical in the case $k>0$, but because this is determined by the fifth-order term, we call the bifurcation degenerate or critical.

It is straightfoward to compute the nontrivial solutions of (A1). There is one unstable periodic orbit for $\lambda_1>0$, and there are two periodic orbits, one stable and one unstable, for

$$-\lambda_2^2/4k < \lambda_1 < 0, \quad \lambda_2 < 0.$$

On the curve $\lambda_1 = -\lambda_2^2/4k$ the two periodic orbits collide in a saddle-node-of-periodic-orbits (SNP) bifurcation. Thus the change in criticality of a Hopf bifurcation is associated with a SNP bifurcation, and the locus of SNP bifurcations has a quadratic tangency with the locus of Hopf bifurcations at the DH.

APPENDIX B: REDUCTION TO AMPLITUDE EQUATIONS

In this appendix we briefly outline how, for the problem at hand, it is, in principle, possible to reduce the dynamics of the streamfunction ψ appearing in the Navier–Stokes equations (1) to the dynamics of two amplitudes.

Assume that for a large class of $\psi(x,y,t)$ including, but not exclusive to, steady and modulated waves, there exists a K such that

$$\psi(x=0,y=0,t) = K \Rightarrow \frac{\partial\psi}{\partial t}(x=0,y=0,t) \neq 0.$$

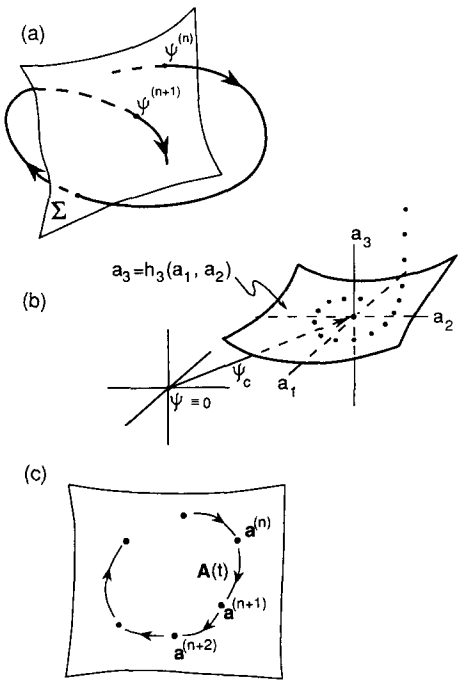

FIG. 10. Diagram illustrating the reduction of the streamfunction ψ in the Navier–Stokes equations to a pair of real amplitudes, A_1 and A_2. (a) Illustration of the Poincaré section used to eliminate the wave speed from the dynamics. The Poincaré section is transverse to the time evolution of the streamfunction. The points $\psi^{(n)}(x,y)$, $\psi^{(n+1)}(x,y)$, etc., are successive crossings of the section in one direction. (b) Diagram illustrating the center manifold on which the asymptotic dynamics takes place. The coordinates of the center manifold are centered on the state ψ_c. The amplitudes of all other modes are slaved to the amplitudes, a_1 and a_2, of the modes ψ_1 and ψ_2. Specifically, the long-time behavior of the amplitude a_3 is given by $h_3(a_1,a_2)$. (c) Illustration of the interpolation of the discrete time amplitudes, $\mathbf{a}^{(n)}$, $\mathbf{a}^{(n+1)}$, etc., by the continuous-time amplitude $\mathbf{A}(t)$. In the figure, $\mathbf{a}^{(n)}=(a_1^{(n)},a_2^{(n)})$, $\mathbf{A}(t)=[A_1(t),A_2(t)]$, etc.

Then the hypersurface Σ given by $\Sigma=\{\psi|\psi(0,0,t)=K\}$ can be used as a Poincaré section for the dynamics [see Fig. 10(a)]. There is nothing special about the point $(x=0,y=0)$, it is simply chosen for concreteness and some other point could be chosen as needed. The Poincaré map Π, taking points on Σ to points on Σ, is given by

$$\Pi:\psi^{(n)}(x,y)\mapsto\psi^{(n+1)}(x,y),$$

where $\psi^{(n)}(x,y)=\psi(x,y,t=T_n)$, with T_n the nth time from $t=0$ such that

$$\psi(x=0,y=0,t=T_n)=K,$$

$$\frac{\partial\psi}{\partial t}(x=0,y=0,t=T_n)>0.$$

The condition that the time derivative be positive ensures that the crossings of Σ in one direction only are considered. [Rather than considering a section transverse to orbits generated by the flow of time, one can consider a section transverse to orbits generated by the symmetry group SO(2), and in this way, collapse to a single point all states that lie on the same group orbit. We choose to consider a Poincaré section transverse to the time flow because such a section can also be used in the absence of symmetry, as in Sec. V.]

Thus we reduce the dynamics of the Navier–Stokes equations to the dynamics of the map Π, and in so doing we remove time explicitly from the problem. In particular, we simultaneously eliminate the wave speed from the dynamics of the steady and modulated waves: steady waves are isolated fixed points of Π and modulated waves lie on an isolated invariant circle for the map. Note that while the Poincaré section in Fig. 10(a) is shown as two dimensional, the section defined by $\Sigma=\{\psi|\psi(0,0,t)=K\}$ is actually infinite dimensional.

The next step is the reduction from the infinite-dimensional Poincaré map to a map of just two amplitudes. For this we need to expand states on the Poincaré section in a set of basis functions. Because we are interested in bifurcations of finite-amplitude waves, we need to consider a coordinate basis for ψ that is centered, not on the point $\psi(x,y)\equiv 0$, but on the nontrivial state ψ_c specified in Sec. III A. Note that if $\psi_c(x=0,y=0)=K$; however, if $K\neq 0$, then $\psi(x,y)\equiv 0$ is not on the Poincaré section.

Given an orthonormal set of basis functions $\{\psi_1(x,y),\psi_2(x,y),\ldots\}$, each of which satisfies $\psi(x=0,y=0)=0$, we can expand the streamfunctions on the Poincaré section $\psi^{(n)}(x,y)$ as

$$\psi^{(n)}(x,y)=\psi_c+\sum_i a_i^{(n)}\psi_i(x,y),$$

where $a_i^{(n)}$ is the amplitude of mode ψ_i at the nth crossing of the section. The Poincaré map Π, then takes the form of a set of modal equations:

$$a_i^{(n+1)}=\Pi_i(a_1^{(n)},a_2^{(n)},\ldots),\quad i=1,2,3,\ldots.$$

As discussed in Sec. III, there are two eigenvalues for the steady waves that are near zero. All the other eigenvalues are bounded away from zero and have negative real part. For the map Π, this means that there are two eigenvalues near $+1$ and all other eigenvalues are inside, and bounded away from, the unit circle. Because of this, we choose the basis functions ψ_1 and ψ_2 to span the two-dimensional eigenspace of the two eigenvalues near $+1$. The time scales of all the other modes are fast in comparison with the time scales of the ψ_1 and ψ_2 modes, and thus the higher modes are slaved to the ψ_1 and ψ_2 modes. Hence, as regards the long-time behavior of the system, it is possible to express the amplitudes of the higher modes as functions of the amplitudes a_1 and a_2:

$$a_3^{(n)}=h_3(a_1^{(n)},a_2^{(n)}),$$

$$a_4^{(n)}=h_4(a_1^{(n)},a_2^{(n)}),$$

$$\vdots$$

The situation is illustrated in Fig. 10(b). Technically, there is a two-dimensional center manifold[8,17,23,24,38] coordinated by the amplitudes a_1 and a_2. Substituting for a_3, a_4,..., we obtain

$$a_1^{(n+1)} = \Pi_1[a_1^{(n)}, a_2^{(n)}, h_3(a_1^{(n)}, a_2^{(n)}), \ldots]$$
$$= \bar{\Pi}_1(a_1^{(n)}, a_2^{(n)}),$$
$$a_1^{(n+1)} = \Pi_2[a_1^{(n)}, a_2^{(n)}, h_3(a_1^{(n)}, a_2^{(n)}), \ldots] \quad \text{(B1)}$$
$$= \bar{\Pi}_2(a_1^{(n)}, a_2^{(n)}),$$

so that the dynamics is contained entirely in the two amplitudes a_1 and a_2. (When parameter dependence is considered, the center manifold is four dimensional, but this in itself presents no difficulties.)

The next stage of the reduction is to bring the equations for a_1 and a_2 into normal form. However, rather than consider normal-form equations for the map, we consider continuous-time normal-form equations. The situation is that, in the vicinity of the degenerate fixed point of interest in this paper, it is possible to approximate the map to any desired accuracy (Ref. 24, p. 311) with a system of differential equations

$$\dot{A}_1 = F_1(A_1, A_2),$$
$$\dot{A}_2 = F_2(A_1, A_2),$$

where the amplitudes A_1 and A_2 are continuous functions of time. The interpolation of the discrete dynamics on the center manifold by continuous amplitudes is illustrated in Fig. 10(c). The amplitudes A_1 and A_2 approximate the amplitudes a_1 and a_2 in the following sense: if the multicritical point is at the origin and if

$$A_1(t = T_n) = a_1^{(n)},$$
$$A_2(t = T_n) = a_2^{(n)},$$

then

$$A_1(t = T_{n+1}) = a_1^{(n+1)} + \epsilon_1,$$
$$A_2(t = T_{n+1}) = a_2^{(n+1)} + \epsilon_2,$$

where ϵ_1 and ϵ_2 go to zero with some power of $|A_1| + |A_2|$. Hence, rather than consider discrete normal-form equations in terms of the amplitudes a_1 and a_2, we consider continuous normal-form equations for the amplitudes A_1 and A_2. From a practical point of view, the center-manifold reduction and the subsequent transformation of the map into normal form are both accurate to some order in the distance away from the degenerate point. Continuous normal forms are constructed to approximate the map normal form to within this same order of approximation.[24,31]

This method of studying bifurcations of maps by means of interpolating flows is a standard approach in bifurcation theory. One typically must worry about the dynamics near homoclinic orbits, because at homoclinic orbits, arbitrarily small perturbations can lead to important qualitative changes in dynamics. However, in the case of the channel, the translational symmetry rules out differences between the map and continuous normal forms that, in the absence of symmetry, occur near homoclinic orbits (Sec. V). Thus, in describing the steady and modulated waves in the plane channel, it is particularly germane to study continuous normal forms rather than normal forms for maps.

[1] S. A. Orszag and A. T. Patera, J. Fluid Mech. **128**, 347 (1983).
[2] B. J. Bayly, S. A. Orszag, and T. Herbert, Annu. Rev. Fluid Mech. **20**, 359 (1988).
[3] J. D. Pugh and P. G. Saffman, J. Fluid Mech. **194**, 295 (1988).
[4] I. Soibelman, Ph.D. thesis, California Institute of Technology, Pasadena, California, 1989.
[5] J.-P. Zahn, J. Toomre, E. A. Spiegel, and D. O. Gough, J. Fluid Mech. **64**, 319 (1974).
[6] T. Herbert, in *Lecture Notes in Physics*, edited by A. I. van de Vooren and P. J. Zandbergen (Springer, Berlin, 1976), Vol. 59, p. 235; AGARD Conf. Proc. CP-224, 1977, p. 3/1.
[7] M. Gorman and H. L. Swinney, Phys. Rev. Lett. **43**, 1871 (1981); M. Gorman, H. L. Swinney, and D. A. Rand, *ibid.* **46**, 992 (1981).
[8] J. E. Marsden and M. McCracken, *The Hopf Bifurcation and Its Applications* (Springer, New York, 1976).
[9] G. Iooss and D. D. Joseph, *Elementary Stability and Bifurcation Theory* (Springer, New York, 1981).
[10] J. Jimenez, Phys. Fluids **30**, 3644 (1987).
[11] The parameter μ is chosen to emphasize the similarity to a recent analysis of convection; see D. Barkley and L. S. Tuckerman, Physica D **37**, 288 (1989).
[12] The references here are too numerous for us to give a complete list. A few examples from diverse areas of research are W. F. Langford, in *Nonlinear Dynamics and Turbulence*, edited by G. I. Barenblatt, G. Iooss, and D. D. Joseph (Pitman, Boston, 1982), p. 215; J. Guckenheimer, Physica D **20**, 1 (1986); G. Dangelmayr and J. Guckenheimer, Arch. Rat. Mech. Anal. **97**, 321 (1987); H. Riecke, J. D. Crawford, and E. Knobloch, Phys. Rev. Lett. **61**, 1942 (1988); Case Study 6 of Ref. 19; Chap. 7 of Ref. 23.
[13] The philosophy of our approach is similar to that of Guckenheimer in Ref. 12, and the reader may find the discussion there of interest. We use the notation of Guckenheimer in labeling bifurcations.
[14] P. G. Saffman, Ann. N.Y. Acad. Sci. **404**, 12 (1983).
[15] B. L. Rozhdestvensky and I. N. Simakin, J. Fluid Mech. **174**, 261 (1984).
[16] F. A. Milinazzo and P. G. Saffman, J. Fluid Mech. **160**, 281 (1985).
[17] D. Ruelle, Arch. Rat. Mech. Anal. **51**, 136 (1973).
[18] D. A. Rand, Arch. Rat. Mech. Anal. **79**, 1 (1982).
[19] M. Golubitsky, I. Stewart, and D. G. Schaeffer, *Singularities and Groups in Bifurcation Theory* (Springer, New York, 1988), Vol. II, and references therein.
[20] F. Takens, Publ. Math. IHES **43**, 47 (1974).
[21] V. I. Arnold, Russ. Math. Surv. **27**, 54 (1972).
[22] R. I. Bogdanov, Funct. Anal. Appl. **9**, 144 (1975).
[23] J. Guckenheimer and P. Holmes, *Nonlinear Oscillations, Dynamical Systems, and Bifurcations of Vector Fields* (Springer, New York, 1983).
[24] V. I. Arnold, *Geometrical Methods in the Theory of Ordinary Differential Equations* (Springer, New York, 1983).
[25] This is not the double-zero eigenvalue discussed by Pugh and Saffman in Ref. 3. The double-zero eigenvalue discussed there results from the degeneracy in the phase of the steady waves. We have eliminated this degeneracy from the problem by considering the dynamics on a Poincaré section as in Appendix B.
[26] M. W. Hirsh and S. Smale, *Differential Equations, Dynamical Systems, and Linear Algebra* (Academic, Orlando, 1974).
[27] I. Soibelman (private communication).
[28] Note that E. Knoblock [Phys. Lett. A **115**, 199 (1986)] has shown that at a double zero with $k_1 = 0$, there is a transformation which makes $k_3 = 0$; however, when λ_1 and λ_2 are nonzero it appears that k_3 must also be nonzero to obtain a sensible unfolding.
[29] There is no contradiction in considering λ_1 large enough for the stability to be determined by the third-order terms, and yet small enough that the third steady state is far from the two steady states of interest. Simply consider λ_1 in the range $k_1^2 < \lambda_1 \ll 1/k_2^2$, which is always possible because we can consider arbitrarily small k_1.
[30] S. Smale, Bull. Am. Math. Soc. **73**, 747 (1967).
[31] G. Iooss, in *Chaos and Statistical Methods*, edited by Y. Kuramoto (Springer, Berlin, 1984), p. 136.

[32] G. E. Karniadakis, B. B. Mikic, and A. T. Patera, J. Fluid Mech. **192**, 365 (1988), and references therein; C. H. Amon and A. T. Patera, Phys. Fluids A **1**, 2005 (1989); M. F. Schatz, R. P. Tagg, H. L. Swinney, P. F. Fischer, and A. T. Patera submitted to Phys. Rev. Lett.
[33] Subharmonic bifurcations produce symmetry breaking and are necessarily of the pitchfork type.
[34] P. S. Marcus, J. Fluid Mech. **146**, 45 (1984).
[35] D. Barkley (unpublished).
[36] R. Seydel, *From Equilibrium to Chaos, Practical Bifurcation and Stability Analysis* (Elsevier, New York, 1988).
[37] Note that in singularity theory, supercritical and subcritical are defined by the direction of bifurcating branches, e.g., M. Golubitsky and D. G. Schaeffer, *Singularities and Groups in Bifurcation Theory* (Springer, New York, 1985), Vol. I.
[38] M. W. Hirsch, C. C. Pugh, and M. Shub, *Lecture Notes in Mathematics* (Springer, Berlin, 1977), Vol. 583.